



# Photoelectrochemical conversion of CO<sub>2</sub> using nanostructured PbS–Si Photocathode

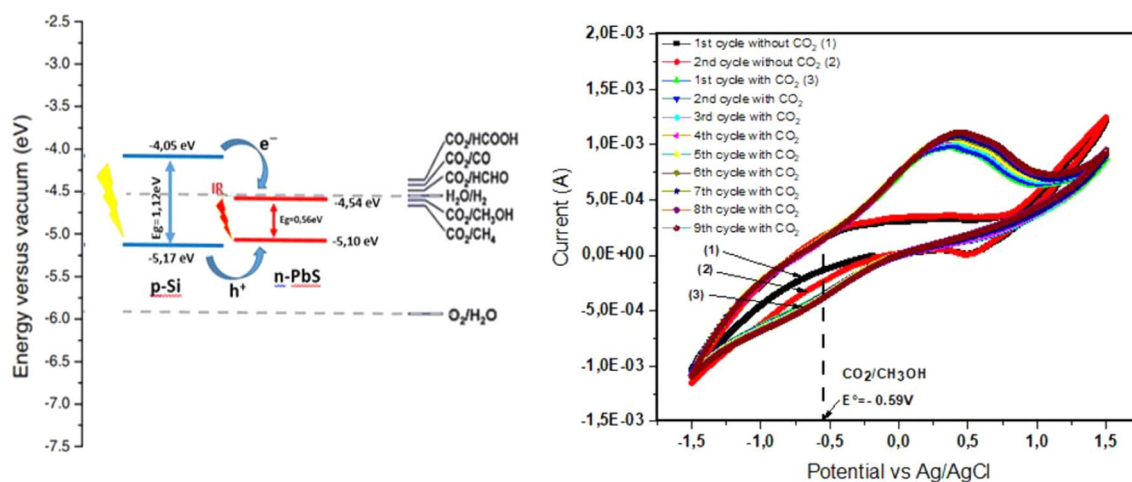
L. Allad<sup>1,2</sup> · D. Allam<sup>2</sup> · K. Benfadel<sup>1</sup> · S. Kaci<sup>1</sup> · M. Leitgeb<sup>3</sup> · A. Ouerek<sup>1,2</sup> · A. Boukezzata<sup>1</sup> · C. Turki<sup>1</sup> · S. Bouanik<sup>1</sup> · S. Anas<sup>1</sup> · L. Talbi<sup>1</sup> · Y. Ouadah<sup>1</sup> · S. Hocine<sup>2</sup> · A. Keffous<sup>1</sup> · S. Achacha<sup>1</sup> · A. Manseri<sup>1</sup> · F. Kezzoula<sup>1</sup>

Received: 25 August 2021 / Accepted: 1 January 2022 / Published online: 15 January 2022  
© The Author(s), under exclusive licence to Springer Nature B.V. 2022

## Abstract

A n-type nanostructured PbS thin films were prepared by chemical bath deposition onto flat Silicon (Si) and Silicon nanowires (SiNWs) which were derived from electroless etching of Si substrates. The morphological characterization was carried out by scanning electron microscopy (SEM), while the optical properties were studied using Ultraviolet–Visible Spectroscopy (UV–Vis). The catalytic activity was studied by linear sweep voltammetry (LSV) in dark and under white light irradiation using potentiostat station. Cyclic voltammetry in presence and without purging CO<sub>2</sub> was also conducted. The LSV investigations showed the coupling effect between PbS thin films and Si for the rising and transport of the charge carriers. The results showed a higher photocatalytic activity toward CO<sub>2</sub> reduction of PbS/SiNWs compared to Silicon substrate without any surface modification and sensitization. The electrode based on PbS/SiNWs/Si could efficiently be used as photocathode for the PEC reduction of CO<sub>2</sub> to Methanol.

## Graphical abstract



**Keywords** PbS/SiNWs/Si · Photocathode · Thin films · Photoelectrocatalysis · CO<sub>2</sub>RR

## 1 Introduction

Nowadays, developing CO<sub>2</sub> transformation via artificial photosynthetic processes constitutes a research area of significant interest; therefore, scientists spare no efforts to find the better way to enable conversion efficiently [1–3]. The

✉ S. Kaci  
kacisamira@crtse.dz; k\_samira05@yahoo.fr

Extended author information available on the last page of the article

photoelectrocatalytic reduction reaction of CO<sub>2</sub> (CO<sub>2</sub>RR) to value-added products may be considered as an economical approach for the energy-dense storage of intermittent renewable electricity. In fact, electric energy can be directly converted to chemical energy by reducing CO<sub>2</sub> in a photoelectrolysis process. Meaningful routes to undergo the CO<sub>2</sub> transformation such as a dry reforming process are usually employed [4–6]. Unfortunately, such procedures usually require high-pressure environments and a considerable amount of thermal energy input. Numerous reviews have been published to discuss the photoelectrocatalytic (PEC) reduction of CO<sub>2</sub>. Hence, the state-of-the-art catalytic systems, the basic principles, and various aspects of the reaction were very well developed and understood [7–12]. However, most of the photoelectrocatalytic processes that have been studied focused on the design of the photoelectrodes and how solar energy is harvested and transferred. This means that efficiency enhancement of solar energy conversion by light harvesting has been the principal theme of numerous papers [13–17]. Actually, the solar driven conversion mechanisms have all in common that for a high product yield efficient light absorption of a semiconductor electrode is necessary which is followed by charge separation due to a space charge region. Therefore, the conception of photoelectrodes that absorb a maximum of solar light and to ensure the separation of photogenerated electrons and holes at the photosynthetic reaction center continue to be an ultimate target that scientists attempt to achieve [18–24].

Generally speaking, the photoelectrocatalytic (PEC) reduction of CO<sub>2</sub> usually requires the presence of a photocatalyst to design the cathode or the anode (depending on the position of the photoelectrode in the electrochemical cell) so that when a bias is applied, CO<sub>2</sub> is reduced at the cathode, with another species (ideally H<sub>2</sub>O) oxidized at the anode. In addition, a photocatalyst should combine the properties of the semiconductor with other new desirable properties which are related to light absorption of the semiconductors. In order to harvest light, an efficient photocatalyst should absorb as much as possible of the wavelengths of the solar spectrum. Nonetheless, this property has not yet been achieved; in fact, the common semiconductors only absorb a meaningless portion of the solar spectrum. Being motivated to hurdle this limitation, light harvesting can be achieved by utilizing cocatalysts having the role of absorbing solar photons and transferring electrons to the semiconductor.

PEC conversion of CO<sub>2</sub> to energetic products employing crystalline silicon Si (c-Si) as photocatalyst-based electrode has been investigated by numerous studies [25–31]. Modifying the surfaces of silicon wafers by nanostructuring is one of the promising ways for enhancing the light harvesting, since the surface-light losses are significantly reduced through photon trapping, enhancing thereby the generated current in the whole PEC process. Beside the

above-mentioned properties, photocathodes of p-Si with integrated cocatalysts have previously been demonstrated to provide light-enhanced CO<sub>2</sub> reduction, with significant faradaic efficiencies.

PbS nanocrystals are of interest because of their strong quantum confinement, due to the large exciton Bohr radius of both electrons and holes (18 nm) [32]. As silicon provides a good platform for integration of the thin film optoelectronic structure into electronic devices, it is a good approach to deposit PbS thin films directly at its surface. PbS/Si heterojunctions have been widely used in optoelectronic devices, in which the Si is used as substrate, while the PbS film serves as IR-absorbing layer [33]. A few reports about the PbS-based heterostructures have been made for photocatalytic applications [34–37]. Employing buffer layers can eliminate the problem related to the lattice mismatch [38]. Nanostructured silicon, including porous and nanowires forms, can be used as a buffer layer [39–41]. All in all PbS/Si structures were investigated in numerous applications [42–44]. But still, no studies reported the use of PbS/Si for either Hydrogen production nor PEC reduction of CO<sub>2</sub>. To address this technology gap, in this work, PbS thin films on Si nanowires were prepared by a combination of aqueous chemical etching of silicon substrates followed by chemical bath deposition of nanostructured PbS thin films in order to evaluate their photocatalytic activity for CO<sub>2</sub> reduction via water oxidation. Our study was motivated by the fact that Si nanowires modified by PbS could lead to an improvement in photocatalytic activity provided that the thickness of PbS layer on the surface of SiNWs is controlled appropriately so that a quick transfer of the electrons and holes from SiNWs to the PbS surface is assured. Based on this, an ultrathin PbS layer for co-catalysis on a SiNWs photocathode was designed and fabricated by using a Chemical Bath Deposition-coating-based method. This ultrathin PbS layer-modified SiNWs photocathode could exhibit highly efficient performance for CO<sub>2</sub> reduction.

This work demonstrates a facile strategy and potential use of low-cost PbS as an efficient cocatalyst with SiNWs for solar methanol production that can be applicable in the general field of energy conversion. Owing to the suitable band alignment between PbS and SiNWs the rapid transfer of photogenerated electrons from the CB of SiNWs to the CB of PbS for selective PEC CO<sub>2</sub> reduction to methanol is facilitated. Thus, to the best of our knowledge, this kind of heterostructure was not investigated elsewhere.

## 2 Experimental procedure

One-step metal-assisted chemical etching process was employed to fabricate the silicon nanowires on p-type Si(100) substrates with a resistivity ranging between 1 and

10  $\Omega$  cm (boron-doped). First, the samples were degreased in acetone and ethanol, rinsed with deionized water, and then dried under a stream of dry  $N_2$ . To remove the native oxide, the samples were immersed in aqueous HF (10%) solution followed by rinsing and drying under a stream of dry  $N_2$ . An aqueous 5 M HF/0.035 M  $AgNO_3$  solution was used for etching the substrates at room temperature for different etching times (60 min and 120 min). Then, the etched samples were dipped in concentrated  $HNO_3$  for 5 min to remove all silver particles. Finally, the samples were rinsed with deionized water and dried under a stream of dry  $N_2$  [45].

PbS thin films were prepared as follows, while samples with size of ( $2 \times 1.5$  cm<sup>2</sup>) were used. Prior to deposition, they were cleaned with acetone in an ultrasonic bath (10 min) followed by washing them in deionized water.  $Pb(NO_3)_2$  (1.35 mmol) was dissolved in deionized water (100 ml), where a transparent solution was obtained. Then, NaOH (8.55 mmol) was added to the solution followed by addition of (102 mol) of thiourea. The synthesis of PbS was carried at room temperature by soaking the cleaned substrates in the deposition bath. Thin films of PbS were deposited on p-Si(100) and SiNWs/Si(100) substrates. [46].

The photoelectrochemical performance of PbS/Si(100) and PbS/SiNWs/Si(100) samples was evaluated through linear sweep voltammetry (LSV) using an AUTOLAB potentiostat with a conventional three-electrode setup. For these electrochemical purposes, the PbS thin films, deposited onto Si(100) and SiNWs-modified Si(100) substrates, were used as working electrode (with an effective area of 3 cm<sup>2</sup>). A Ag/AgCl (3.5MKCl) was used as reference and platinum wire as counter electrode, respectively. The electrolyte was 0.01 M  $K_2CO_3$  solution. In order to calculate the flat band potential ( $E_{fb}$ ) of the films in the range from  $-1.5$  to  $0.5$  V vs Ag/AgCl (3.5MKCl), we conducted the electrochemical measurements in dark and under artificial visible light delivered by a lamp with a power of 70 W.

The  $CO_2$  reduction reaction ( $CO_2RR$ ) measurements were performed in an airtight one-compartment electrochemical cell under ambient temperature and solar room lightning. The compartment consisted of PbS/SiNWs/Si as the working electrode, Ag/AgCl (3.5 M) as the reference electrode, and the platinum wire as the counter electrode. 0.01 M aqueous  $K_2CO_3$  was used as the electrolyte and was saturated with  $CO_2$  for 30 min which was generated by making mixtures of (sugar + baking powder + warming water). The generated  $CO_2$  gas was bubbled into water continuously with a uniform velocity (10 sccm). The photoelectrocatalytic measurements were carried out by sweeping the potential from  $-1.5$  to  $+1.5$  V for 1 h (10 cycles). The liquid phase products were analyzed by GC measurements. The samples were analyzed using Gas Chromatography equipped with a thermal conductivity detector.

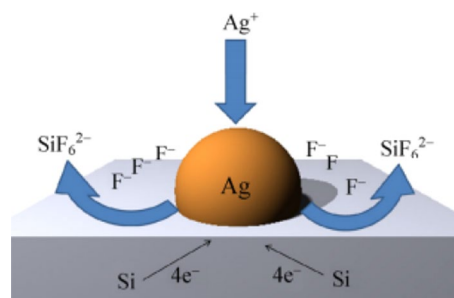


**Fig. 1** A schematic of the electroless metal deposition process. (Color figure online)

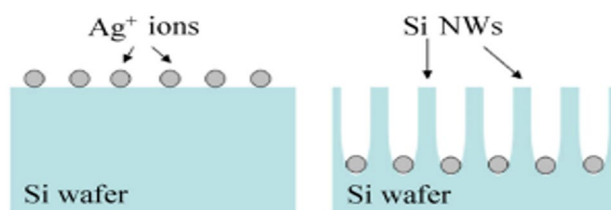


**Fig. 2** A schematic of Ag-assisted etching process of Si surface to form the Si NWs. (Color figure online)

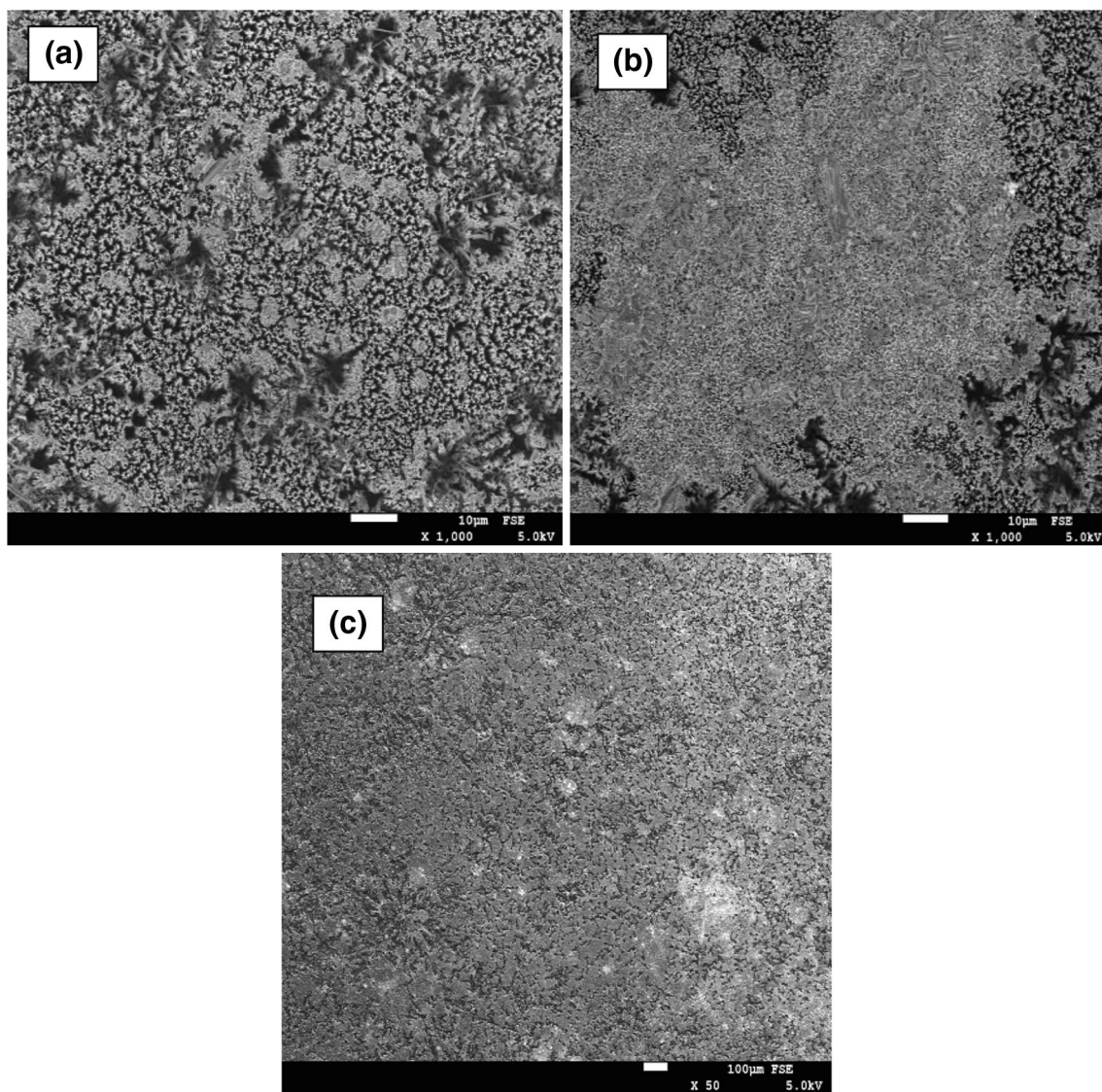
## 3 Results and discussion

### 3.1 Formation of silicon nanowires and PbS deposition

Metal-assisted etching involves metal deposition on a Si substrate from a metal ion containing a HF solution. Figure 1 shows an Ag particle deposited on the Si surface prior to etching. Metal deposition is a localized chemical redox process in which both anodic reaction (Si oxidation) and cathodic one ( $Ag^+$  reduction) occur simultaneously at the Si surface [47].

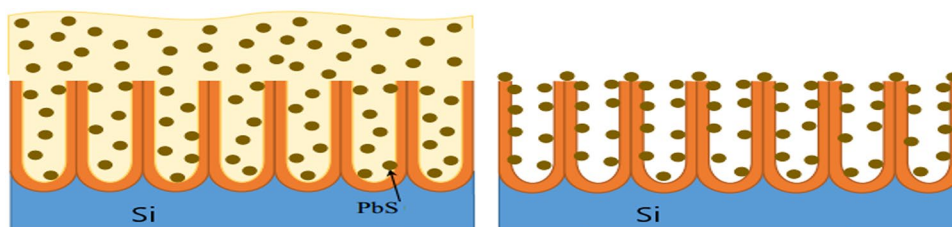
Si oxides are etched by HF and dissolved in aqueous solution. The etching mechanism begins with the electroless deposition of Ag particles on the Si substrate. Firstly, electrons of the Si are captured from its valence band by  $Ag^+$  ions and are reduced to Ag nuclei. Secondly, the Si hexafluoride anion ( $SiF_6^{2-}$ ) is formed by oxidation of the Si directly under the deposited Ag particles and subsequent dissolution of the oxide by HF. The metal particles then etch through the Si and the remaining sidewalls form the Si NWs as shown in Fig. 2.

Figure 3a shows the SEM micrograph of the prepared Si NWs. The nanowires are distributed over the whole surface of the sample. Figure 4a shows the long Si nanowires. Figure 4b shows the SEM image of the PbS nanocrystalline thin film prepared on the SiNWs/Si(100) substrate by the CBD method. The PbS starts to grow locally at the



**Fig. 3** SEM observations of SiNWs (etching time = 2 h) and modified Si(100) substrates **a** before and **b, c** after PbS thin film deposition. (Color figure online)

**Fig. 4** Schematic process of PbS deposition on a SiNWs surface (the orange region supposed to be native  $\text{SiO}_2$ ). (Color figure online)



silicon nanowires until it covers their whole surface (see Fig. 3c). A schematic presentation of the PbS deposition on SiNWs is given in the Fig. 4.

Promoting light absorption by photocathodes is an ultimate target to achieve. The light absorption capability of photocathodes is intrinsically determined by the optical

property of the semiconductors. Given the same choice of semiconductor material, its light absorption could be enhanced by surface texturing or electrode nanostructuring. Many photoelectrodes are prepared based on bulk semiconductors with planar and smooth surface, which typically exhibit limited photocurrent density because of severe light

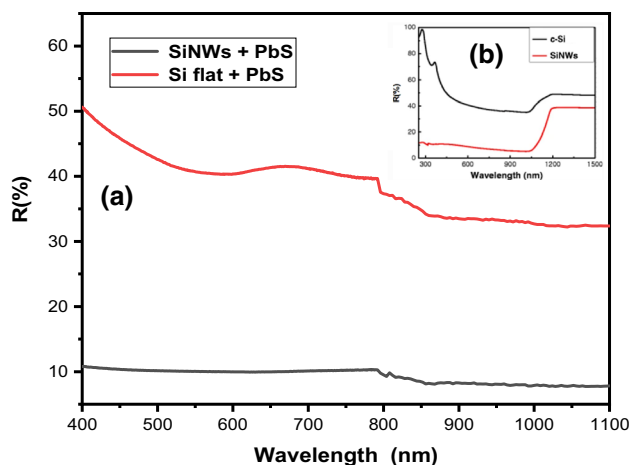


**Fig. 5** Reflectance spectra of flat silicon and SiNWs. a both recovered with PbS thin film and b without PbS deposition. (Color figure online)

reflection on planar surface. For example, the reflectance of a typical polished Si wafer is 25–60% over a wide spectrum from 350 to 1100 nm. When subjected to surface nanostructuring, the surface of Si substrate can be engineered to form nanostructures for trapping the incident light, thereby reducing the light reflectance. Also, light harvesting by a single semiconductor material is sometimes limited. Adding another complementary light-absorbing material in addition to the semiconductor may enhance the overall light-harvesting capability and has been proved as an effective strategy recently. Silicon is a popular p-type semiconductor material for PEC CO<sub>2</sub> reduction, but has limited light absorption. An approach to overcome this limitation consists on the fabrication of SiNWs-coated PbS array photocathodes (Fig. 5). PbS has a much narrower bandgap of ~0.56 eV. Its incorporation here extended the light absorption range of the photocathode. Moreover, the proper band alignment between PbS and SiNWs facilitated the rapid transfer of photogenerated electrons from the CB of SiNWs to the CB of PbS for selective PEC CO<sub>2</sub> reduction to methanol.

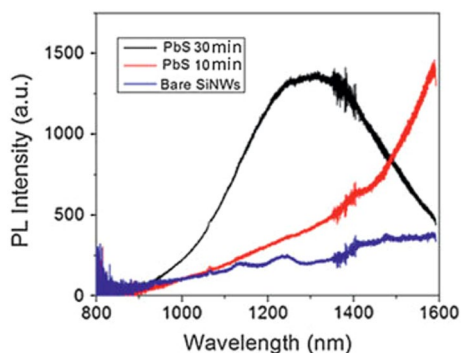


**Fig. 6** PL spectrum of SiNWs-coated PbS thin film. (Color figure online)

Figure 5 shows the total reflectance spectra of SiNWs and the flat-Si substrate both covered with PbS thin film. The total reflectance of flat-Si/PbS (figure inside) demonstrates the well-known behavior of the wafer, the reflection value of ~30% for the range of the strong absorption ( $\lambda < 1 \mu\text{m}$ ), and for the transparency region ( $\lambda > 1 \mu\text{m}$ ), the reflection value increases because of both side contributions. Also, SiNWs exhibit a strong decrease of the total reflectance to 5–10% in the spectral region  $\lambda < 1 \mu\text{m}$  in comparison to the flat-Si substrate (figure inside). It is clearly seen that covering both silicon surfaces with PbS thin film broaden further the wavelength absorption in the IR spectral region, the sample with SiNWs/PbS looks similar to “black silicon”, and its antireflection property can be beneficial in photoelectrocatalytic applications. The strong light scattering and absorption, which results in partial localization (trapping) of the excitation light in SiNWs/PbS arrays, could enhance the photoelectrocatalytic activity when it is used as photoelectrode.

Figure 6 shows the typical spectra of the interband PL, for comparison, of bare SiNWs substrate and SiNWs/PbS samples for different time deposition. Photoluminescence (PL) spectra for bare SiNWs (blue), 10 min of CBD PbS (black), and 30 min of CBD PbS (red). The ability to uniformly coat nanowires with a single layer of PbS nanoparticles allows for a unique way to tune the optical properties of these materials by simply controlling the time of CBD layer.

## 3.2 Energy diagram and band position of PbS/Si

In an attempt to construct the band diagram energy of the studied heterostructure, we have used the diffuse reflectance of the PbS/Si in order to determine the bandgap energy of the PbS thin film which was estimated, employing the Kubelka Munk relation [48], to be equal to 0.56 eV. Regarding what was reported in previous studies, the mean grain size of PbS particles corresponding to 0.56 eV is about 10 nm [34]. The relationship between the bandgap of PbS QDs and particle size is summarized in Fig. 7.

### 3.2.1 Flat band determination

This paper deals with the energetics (bandgap, band energies) of PbS thin films. To decide what photoelectrochemical processes are possible at a semiconductor/liquid interface, one must know the magnitude of the bandgap energy ( $E_{bg}$ ), the relative energies of the band edges, and the location and density of states within the gap.  $E_{bg}$  is usually measured by spectroscopic and/or electrochemical methods. The band edges are usually located energetically by determination of the flat band potential ( $V_b$ ), which can be estimated at single-crystal semiconductor electrodes by capacitance measurements (Mott-Schottky plots) or by the potential dependence of the photocurrent.

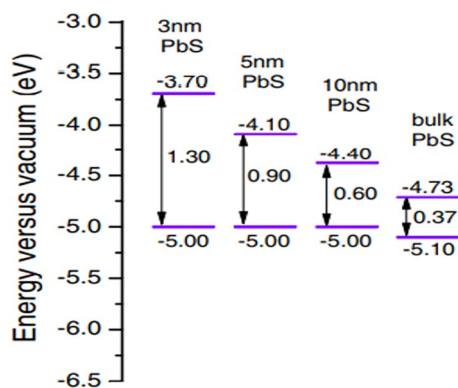


**Fig. 7** The relationship between the bandgap of PbS and particle size. (Color figure online)

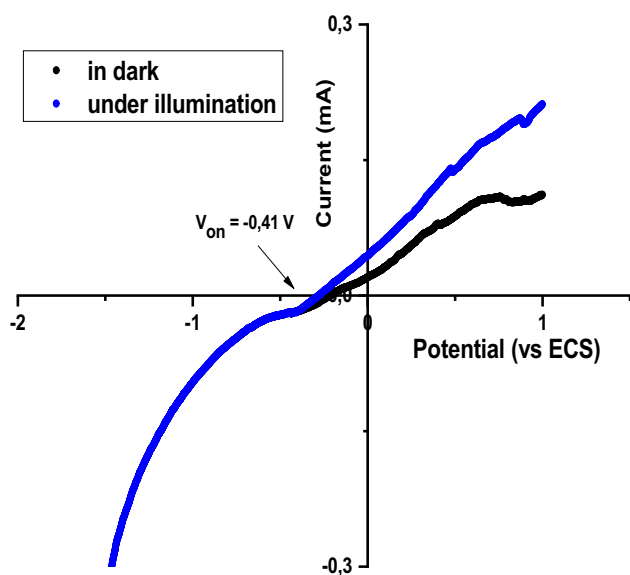


**Fig. 8** LSV curve of PbS pellet in aqueous KOH solution (0.1 M). (Color figure online)

The flat band potential ( $V_{fb}$ ) was determined by plotting I–V curves both in the dark and under illumination (Fig. 8). The increase of the photocurrent ( $J_{ph}$ ) toward the anodic direction confirms the n-type conductivity of PbS. In KOH media,  $J_{ph}$  starts to flow at a potential  $V_{onset}$  of  $-0.41$  V and increases until saturation. We found the type of conductivity of the deposited PbS thin film electrochemically by carrying out LSV with a PbS sample in dark and under illumination. The obtained PbS thin film has an « n » type conductivity.

The linear plot of  $I_{ph}^2$  intercept the potential axis gives the flat band potential  $E_{fb}$ . The energies of the valence (EVB) and conduction bands (ECB) of a material are of great importance in applied photocatalysis and valuable information can be extracted from the PEC characterization. Their

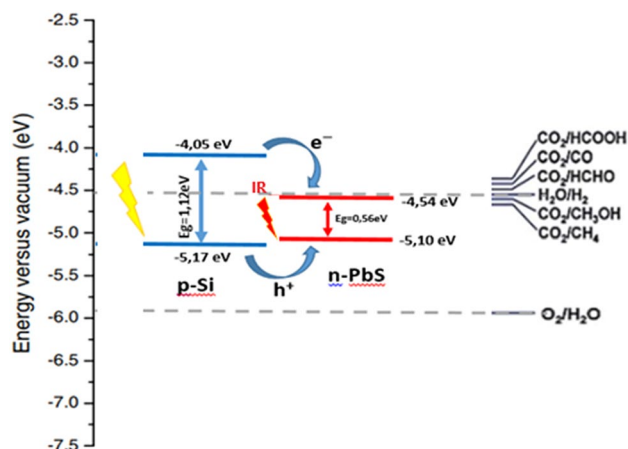


**Fig. 9** Energy diagram illustrating the band energy positions of PbS/Si heterostructure. (Color figure online)

knowledge allows the energy diagram construction of the different band energy position of the studied material.

They can be determined using the following relations:

$$ECB = -4.75 + e V_{fb} + E_a,$$

$$EVB = ECB - E_g,$$

where  $-4.75$  eV represents the potential of the reference electrode (SCE) vs vacuum and  $E_a$  is the activation energy which is the difference between conduction bands and Fermi level. For  $E_g$  of  $0.56$  eV, we found the following:  $ECB = -4.54$  eV and  $EVB = -5.10$  eV.

As can be seen from Fig. 9, the Si valence band edge is obviously below the PbS band edge, which satisfies the energetic requirement for hole transfer. Moreover, the Si conduction band is higher than that of PbS; hence, for contact formation, the electrons will be transferred from the Si to PbS until a thermodynamic equilibrium is established. This will result in the formation of an electron depletion region and surface upward-bent band in Si to facilitate electron and hole transfer.

The PbS/electrolyte interface is equivalent to a double electrochemical layer which behaves like a capacitor of capacitance  $C_{dc}$ , (Gouy-Chapman model).

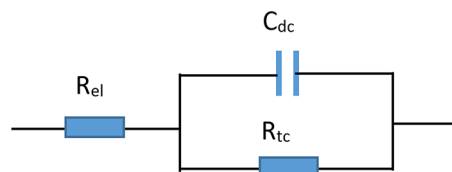


**Fig. 10** Equivalent electrical Circuit of the PbS/0.1 M KOH interface. (Color figure online)

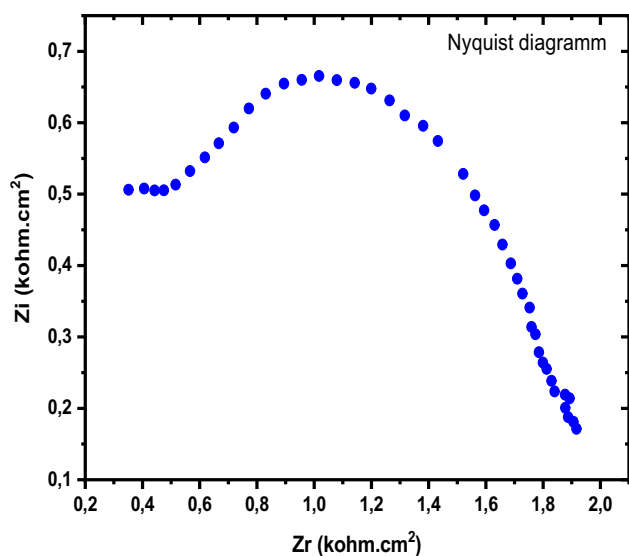


**Fig. 11** Equivalent electrical Circuit of the PbS/0.1 M KOH interface. (Color figure online)

Electrical impedance of this interface is calculated by mean of complex impedance  $R//C$  circuit (mounted in parallel):

$$Z = 1 / (1/R + iwC)$$

where  $\omega$  (rad/s) is pulsation and  $i$  is the imaginary number ( $i^2 = -1$ ).

The Nyquist impedance curve is carried out using potentiostat equipped with an impedance meter, the same which is used for ( $I-V$ ) measurements, with a broad range of frequencies. The curve allows the obtention of the charge transfer resistance ( $R_{tc}$ ), the capacity of the double layer ( $C_{dc}$ ), and the electrolyte resistance ( $R_{el}$ ), corresponding to our system PbS/electrolyte which can be simulated by the equivalent electrical circuit equivalent given in Fig. 10.

Nyquist curve consists of plotting the imaginary part of the impedance as function of the real part in orthonormal system. Half-circle diameter is equal to the resistance  $R_{tc}$  and the pulsation at the maximum is equal to  $\{R_{tc} C_{dc}\}^{-1}$  (see Fig. 11).

The shifting from origin corresponds to the electrolyte resistance ( $R_{el} \sim 350 \Omega \text{ cm}^2$ ) weak for a KOH solution because of the high mobility of  $\text{OH}^-$  ions ( $190 \Omega/\text{cm mol}$ ).

### 3.3 Photoelectrocatalytic properties

The photoelectrocatalytic properties were first tested toward water splitting in absence of  $\text{CO}_2$ . Fig. 12 shows the LSV tests for the two PbS/SiNWs/Si-based working electrodes, in dark and under artificial visible light, for different SiNWs samples. As can be seen, at  $-1 \text{ V}$  vs Ag/AgCl (the

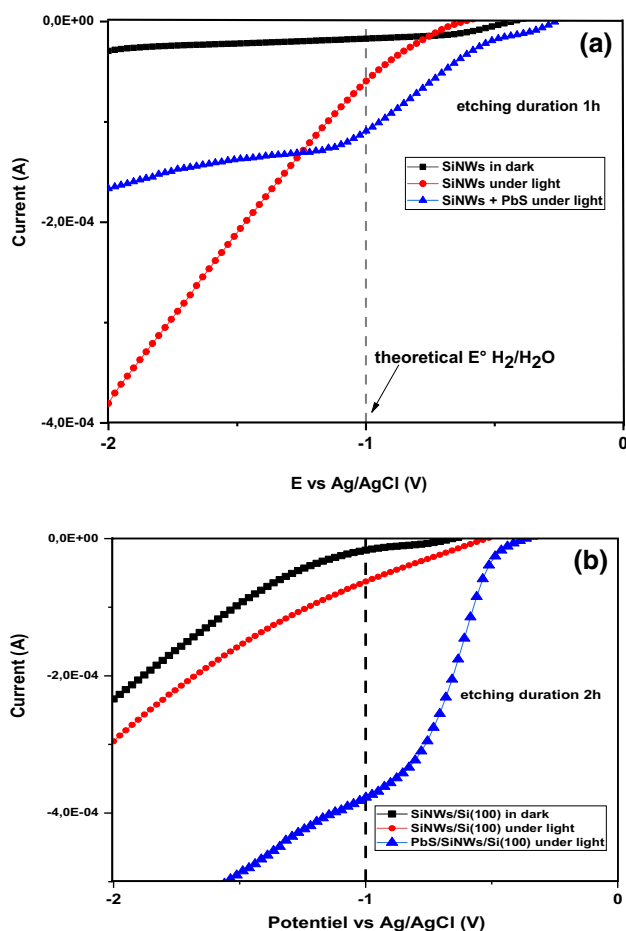


**Fig. 12** LSV of SiNWs/Si(100) and PbS/SiNWs/Si(100)-based working electrodes, as function of etching time **a** for nanowires of 1H and **b** for nanowires of 2H, in dark and under illumination in  $10^{-2}$  aqueous  $\text{K}_2\text{CO}_3$ . (Color figure online)

theoretical potential necessary for water reduction), the generated cathodic photocurrent for the SiNWs/Si(100) in dark is negligible compared with the cathodic photocurrent of the PbS/SiNWs/Si(100)-based electrode. It shows also a higher photocurrent than the SiNWs electrode under illumination which is due to the synergy between the PbS nanoparticles and SiNWs to generate charge carriers for water splitting. Additionally, the photocurrent of PbS/SiNWs/Si(100) electrode, with nanowires that were obtained after 2 h of etching, was improved with respect to the PbS electrode with lower etching time nanowires, which means that the electron–hole transport to the surface was improved. This observation is consistent with the fact that PbS/SiNWs/Si dispose of a wide range of the light spectrum, as was observed in the reflectance spectra (which was not reported here).

From these results, it is theoretically possible to photoelectrochemically reduce carbon dioxide to methanol and or formate, even if the  $\text{CO}_2/\text{methanol}$  reduction potential

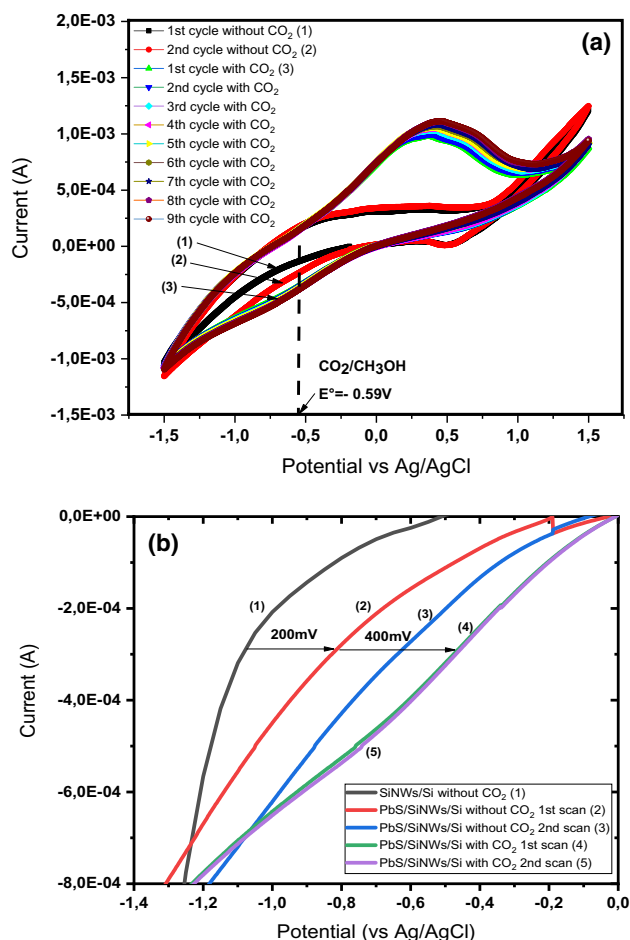
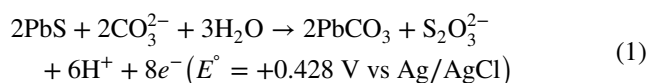


**Fig. 13** **a** Cyclic voltammograms (10 mV/s) of a freshly prepared PbS/SiNWs/Si photocathode in 0.01 M  $\text{K}_2\text{CO}_3$  under light and after 30 min of  $\text{CO}_2$  bubbling which show the successful reduction of  $\text{CO}_2$ . **b** Detailed cathodic current of the cyclic voltammetry curves. (Color figure online)

is only 20 mV positive below that of water, which would indicate a competition of  $\text{CO}_2\text{RR}$  with hydrogen generation. But, the studied working electrodes based on PbS/SiNWs/Si have a high hydrogen overpotential which allows the reduction reaction of carbon dioxide to achieve high selectivity toward  $\text{CO}_2\text{RR}$ .

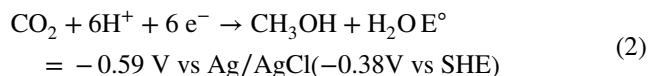
### 3.4 Investigations of PbS/SiNWs/Si photocathodes for $\text{CO}_2$ reduction reaction

The cyclic voltammograms (CVs) of the PbS/SiNWs/Si are shown in Fig. 13. On a freshly prepared electrode, a distinct oxidation peak is present in the first anodic scan under  $\text{CO}_2$ -saturated conditions (pH = 10), corresponding to the oxidation of PbS species to  $\text{Pb}_{1-x}\text{S}$  [49] as is given in the following equation:



A formation of a metastable sulfur-rich sulfide underlayer is supposed to occur at the initial oxidation stage, yielding a monolayer of  $\text{PbCO}_3$  in alkaline solutions [49]. It is interesting that the oxidation peak appears when the solution was saturated with  $\text{CO}_2$ , indicating that the oxidation of PbS particles is related to  $\text{CO}_2$  or  $\text{CO}_3^{2-}/\text{HCO}_3^-$ . The peak remains unchanged in the following scans. Moreover, with  $\text{CO}_2$ , an enhanced cathodic current is observed at potentials  $\leq -0.5$  V (vs. Ag/AgCl electrode), which demonstrates that the  $\text{CO}_2$  is effectively reduced [50]. Also the influence of PbS particles was evidenced through the enhanced the photocatalytic activity of the photocathode after decorating SiNWs with the sulfide. Hence, the shift toward positive potential values after addition of PbS nanoparticles was observed (see Fig. 8b). An enhancement of 200 mV was noticed. The same effect was noticed after saturating the solution with  $\text{CO}_2$ . A shifting of about 400 mV was observed which confirm the photocatalytic activity of the working electrode toward  $\text{CO}_2$ .

As seen in this figure, the same current density can be achieved with a lower applied potential when the electrolyte is saturated with  $\text{CO}_2$ . This indicates the conversion of  $\text{CO}_2$  to methanol instead of hydrogen generation since the thermodynamic potential for photoelectrochemical reduction of  $\text{CO}_2$  to  $\text{CH}_3\text{OH}$  in the presence of protons is generally explained by the following equation and its corresponding reduction potential:



Considering the positive oxidation state(s) of metal centers, in conjunction with the facile removal of chalcogenide anions in aqueous solutions, a Pb layer could be achieved through onsite electrochemical oxidation of PbS during  $\text{CO}_2\text{RR}$  [50]. Previous studies reported that during photoelectrocatalysis, the nanocrystalline PbS was reduced to Pb and it is demonstrated that during the PbS-to-Pb transformation, a new phase of  $\text{PbCO}_3$  was initially generated from the equilibrium  $\text{S}^{2-}/\text{CO}_3^{2-}/\text{HCO}_3^-$  anion exchange, and  $\text{PbCO}_3$  was the primary source to trigger the formation of Pb thin films [51]. The PEC stability of the SiNWs/PbS-based photocathodes was evaluated by chronoamperometry measurements at fixed potential of  $-0.6$  V for 60 min (Fig. 14). The stability of the photoelectrodes shows a gradual degradation from the beginning until 1500 s after that remains stable during the rest time. The deterioration of the photocathode was caused by the photocorrosion of the PbS layer with



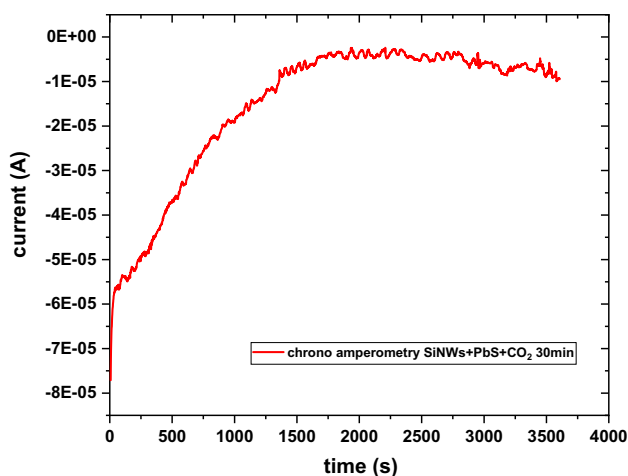


**Fig. 14** I-t curve of SiNWs/PbS-based electrode for fixed voltage of  $-0.6$  V for 60 min. (Color figure online)

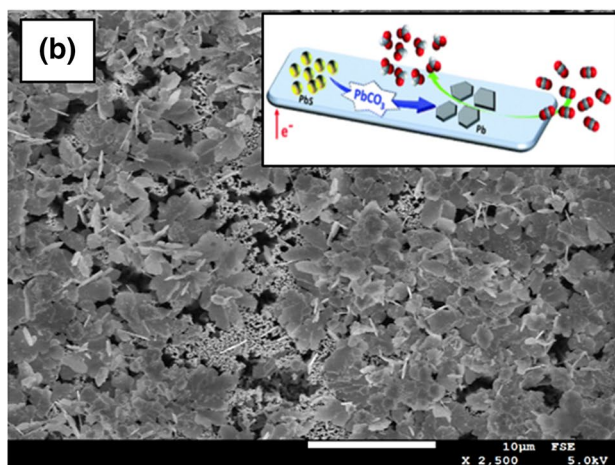
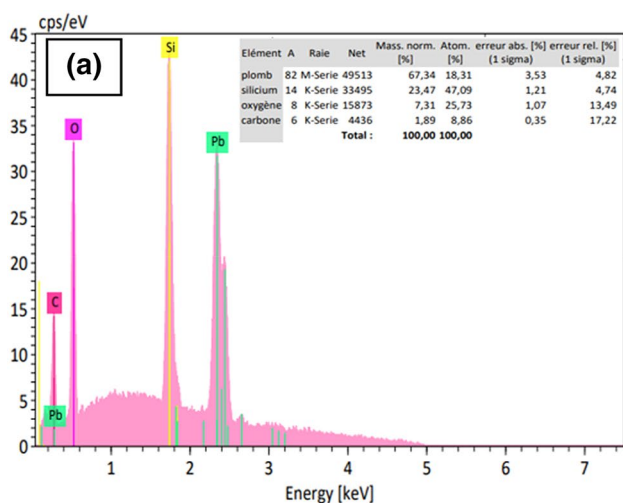


**Fig. 15** **a** EDX and **b** SEM analysis of the surface of the working electrode PbS/SiNWs/Si after  $\text{CO}_2\text{RR}$ . (Color figure online)

apparition of new Pb layer as it was attested by the EDX elemental mapping (Fig. 15b).

Figure 15 shows the EDS analysis and the corresponding SEM micrograph of the surface of the working electrode used for  $\text{CO}_2\text{RR}$  at the end of the reaction. It can be seen that sulfur « S » had disappeared and one can only see lead « Pb » remained, which means that the PbS was effectively turned to Pb during the  $\text{CO}_2\text{RR}$ . Some carbon element atoms were detected on the surface, which supports the results previously reported in ref [51].

For a practical system, chemical stability is a critical issue for realizing large-scale implementation of solar energy conversion. Many semiconductors, such as metal sulfide materials, silver/containing compounds, copper-based materials, zinc oxide and so on exhibit relatively low chemical stability due to light-induced photocorrosion. For instance, metal sulfide-based photocatalysts are susceptible to corrosion under illumination, during which the surface sulfide ions ( $\text{S}^{2-}$ ) are oxidized by photogenerated holes to form sulfate ( $\text{SO}_4^{2-}$ ) and/or sulfur ( $\text{S}^0$ ) depending on whether or not molecular oxygen is present, thus resulting in deactivation of the photocatalyst.

To date, numerous efforts have been devoted to restraining the photoinduced instability of semiconductor with a focus on parameters such as modifying the crystal structure, size, and morphology of semiconductors, doping with anions and/or cations, combining with other semiconductors, hybridizing with various cocatalysts, and tuning the conditions for different reaction systems.

In the case of PbS particles, an attempt consisting on capping them with thiols has been investigated and the results revealed that this approach could enhance the photostability in the near-IR spectral range. This was reported in the study conducted by Xusheng Zhao et al. [52] whose synthesized Thiol-capped water-soluble PbS nanocrystals (NCs) stabilized with 1-thioglycerol, dithioglycerol, or a mixture of 1-thioglycerol/dithioglycerol (TGL/DTG) which were prepared via one-stage synthesis at room temperature. We found that NCs stabilized with a TGL/DTG mixture and show efficiency and good photostability in the second “biological window” (1050–1200 nm).

Other explanation regarding the photogenerated-hole-induced instability metal sulfides must be taken into account. Indeed, upon suitable light illumination, electrons and holes are generated from the conduction band (CB) and valence band (VB), respectively. Photoexcited electrons are smoothly transferred to the surface, while the transfer of holes is problematic. The photogenerated holes could be enriched on the outer surface of a metal sulfide photocatalyst before being consumed by electron donors in the reaction system. Under such circumstances, photocorrosion originating from irreversible hole-driven oxidation reactions in metal sulfides has frequently been observed,

leading to the oxidation of surface sulfide ions ( $S^{2-}$ ) to sulfur ( $S^0$ ) and/or sulfate ( $S_2O_3^{2-}$ ), thereby resulting in low photostability of metal sulfides that greatly restricts their practical applications. Therefore, excess of photoinduced holes which accumulate on the surface of metal sulfide is the principle source of photodissolution [53]. FTIR spectra of PbS films are displayed in Fig. 16. The main spectral features are similar, excepting the intensity of the absorption band of  $CO_3^{2-}$  at  $\sim 1384\text{ cm}^{-1}$ ; the band located at  $\sim 1921\text{ cm}^{-1}$  was assigned to be one of the fundamental frequency of  $COO^-$  bonds. The broad absorption band at the  $\sim 3423\text{ cm}^{-1}$  region can be attributed to stretching of the -OH groups of defective sites and the physically adsorbed water molecules. The band at  $\sim 1018\text{ cm}^{-1}$  was ascribed to the vibration of amine groups. The peaks at  $\sim 2341$  and  $\sim 2369\text{ cm}^{-1}$  are characteristic of  $COO^-$  stretching vibrations, confirming the presence of acetate ions which indicate the bonding to the surface of PbS by the carboxyl groups. The Pb-S bond is mainly an electrovalent bond; thus, the FTIR spectrum of PbS does not show strong bands associated with Pb-S stretching and bending vibration. The bands at  $\sim 780$  and  $\sim 920\text{ cm}^{-1}$  were not identified, but may be associated with Pb-O bond. These spectra clearly do not show peaks corresponding to  $CH_3-COO^-$ ,  $OH^-$ , and  $CO_3^{2-}$  ions which are supposed to remain on the surface of nanocrystals, which means that they were removed by washing with distilled water and drying the films with dry  $N_2$  flow.

Figure 17 shows the characteristic peaks of a Gas Chromatograph for the electrolyte before and after  $CO_2RR$  and for the pure Methanol which was used as standard to allow the different concentration calculations. As we can see,

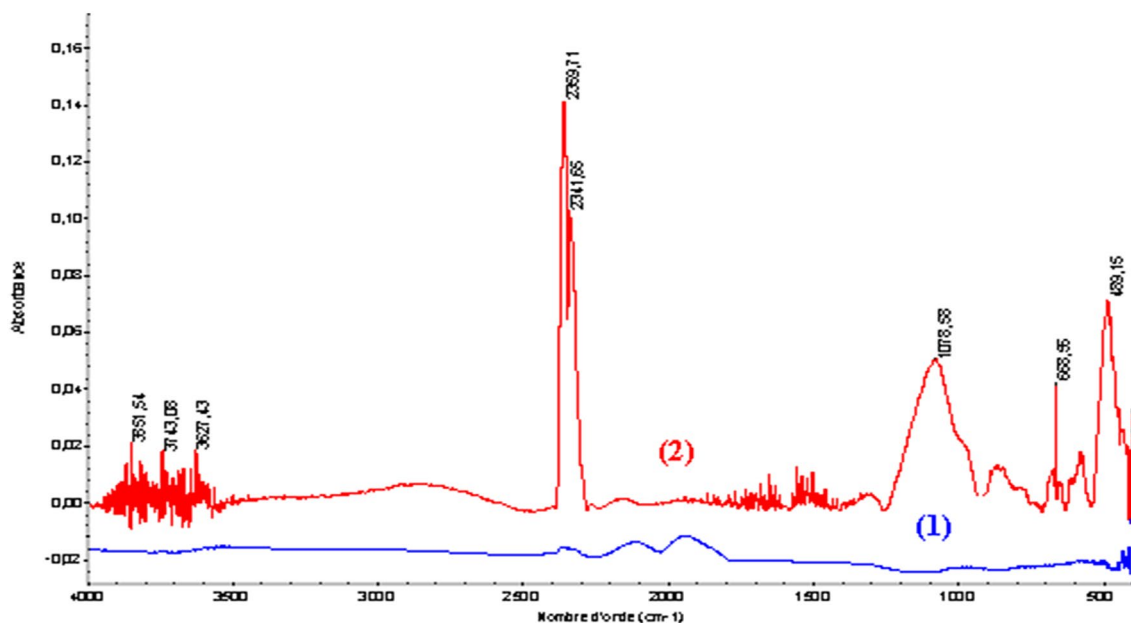


Fig. 16 FTIR analysis of electrode's surface before (1) and after (2) photoelectrochemical investigation. (Color figure online)

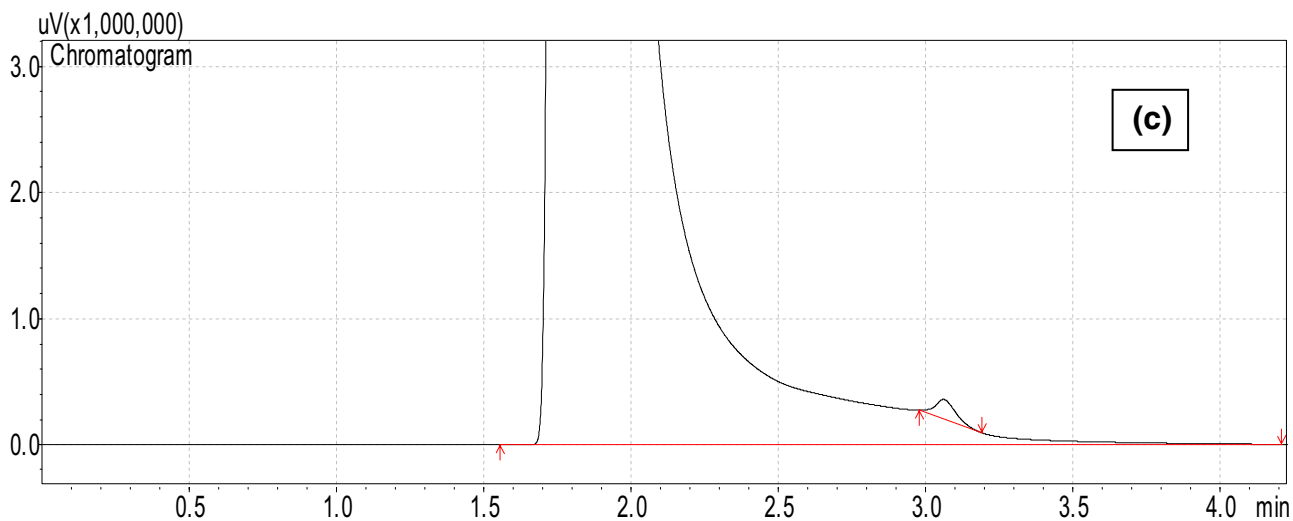
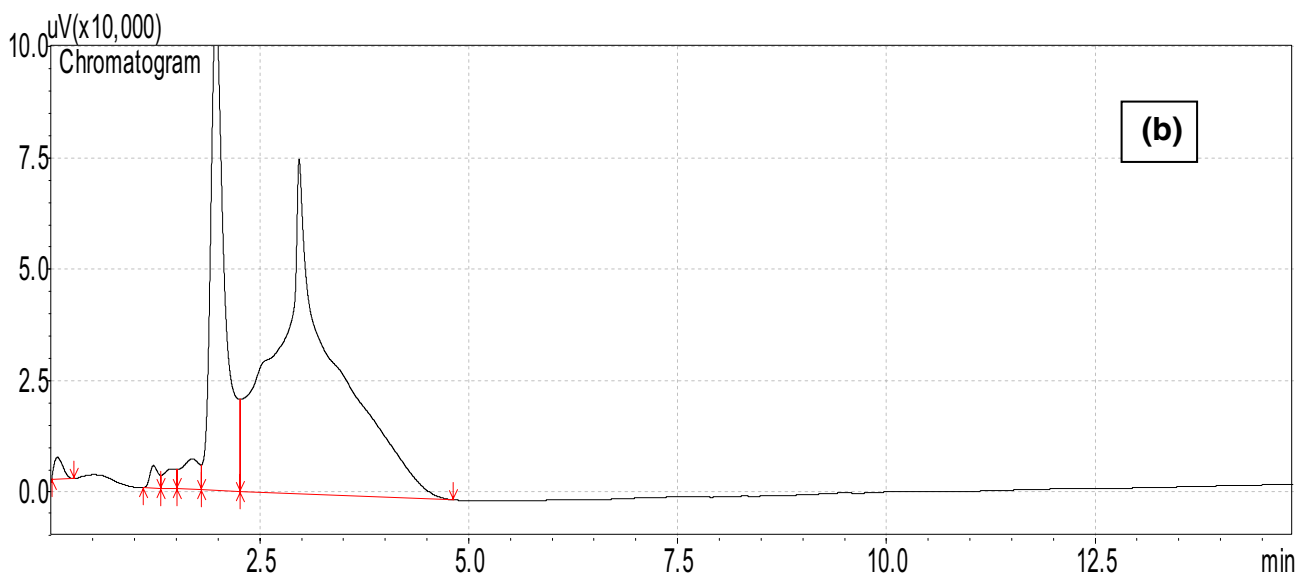
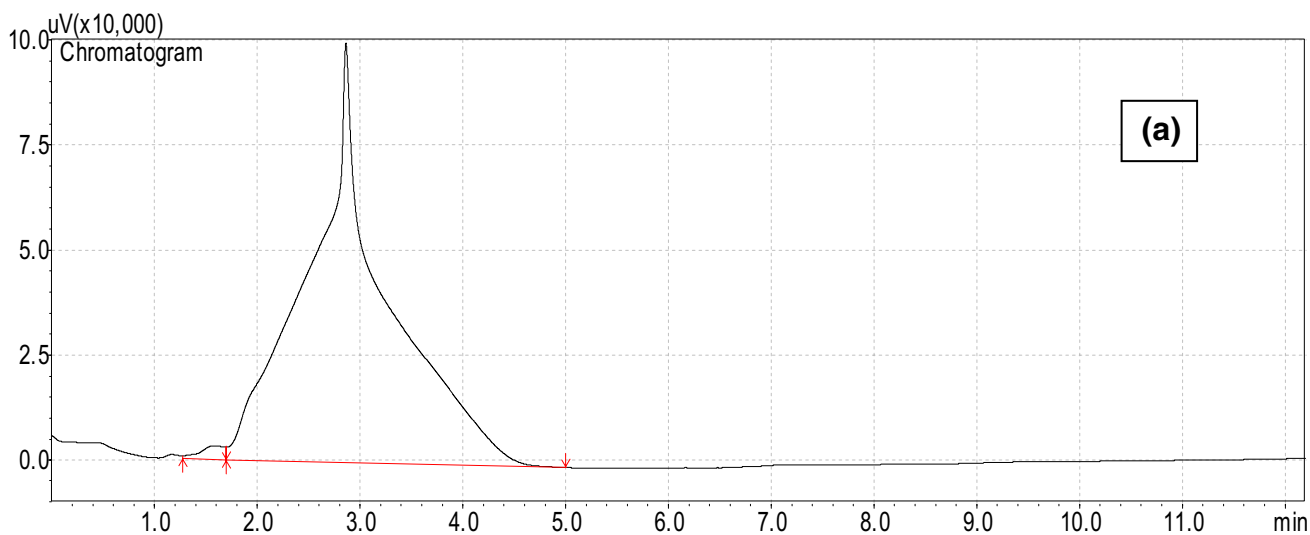
Fig. 17 Characteristic peaks of a Gas Chromatograph of **a** electrolyte before  $CO_2$  reduction, **b** electrolyte after  $CO_2$  reduction and **c** pure methanol. Approximate peak time for methanol: 2 min. (Color figure online)

methanol was detected as one of the main products among the multiple other products of  $CO_2RR$  in very small concentrations compared to that of methanol. This is in accordance with the constructed energy diagram of band energy positions of Si and PbS in which, the CB of PbS was well positioned to allow the reduction of  $CO_2$  to methanol instead of other products and electron transfer increased by the enhanced light absorption of silicon nanowires that makes the reduction easy thanks to the availability of sufficient electron to allow the transformation of  $CO_2$  to Methanol according to Eq. 2.

The consumption of electrons during the reduction of  $CO_2$  is associated by the utilization of produced holes for anodic oxidation of PbS to  $PbCO_3$ , hence, the photocorrosion is avoided and a thin film of Pb is produced on the surface of the SiNWs which plays itself the role of electrocatalyst as explained previously. The electrode based on PbS/SiNWs/Si could be used as photocathode for the PEC reduction of  $CO_2$ .

### 3.5 Solar-to-fuel (STF) efficiency

The solar-to-fuel (STF) efficiency describes how efficiently solar energy is converted to chemical energy (products). It can be calculated from the following equation [54]:



$$\eta_{\text{STF}} = \frac{\Delta G \times n}{P \times A \times t} \times 100 \quad (3)$$

In this equation,  $\Delta G$  is the standard Gibbs free energy of the product,  $n$  is the amount of product in mol,  $P$  is the power density of the light source, where  $DG$  is the product's standard Gibbs free energy of the formation,  $P$  is the light illumination power density,  $S$  is the geometric area of the photoelectrode, and  $t$  is the PEC reaction time. An efficiency of about 4.28% was calculated based on the following information: concentration of pure methanol in 0.2  $\mu\text{l}$  381,790,452 ppm. Daylight power 200 W, electrode Area of 2.25  $\text{cm}^2$ , reaction time of 3600 s,  $AG^\circ = 29$  kJ/mol for methanol formation in aqueous solution.

The characterization evolved here by the gas chromatography was that of the methanol converted from  $\text{CO}_2$  after 1 h. By analyzing the results, we think that the reduction does not reach yet the maximum, after this small time interval, but we cannot be sure as we have not investigated the amount of methanol produced for more than 60 min to clearly see the maximum. An evidence is that, the efficient conversion of  $\text{CO}_2$  to methanol is possible due to the suitable conduction band (CB) edge potential of the PbS semiconductor which indicate that the photogenerated electrons possess enough energy to reduce  $\text{CO}_2/\text{CO}_3^{2-}$  into methanol molecules. Meanwhile, it is important to bear in mind that a pair of competitive reactions (i.e., photoelectrocatalytic reduction and photoelectrocatalytic oxidation) might take place in our photoelectrocatalytic reduction of  $\text{CO}_2$ . According to our results, a low concentration of methanol is produced, and the reaction rate of the photoelectrocatalytic reduction of  $\text{CO}_2$  ( $k_{\text{pecr}}$ ) seems to be faster than that of photoelectrooxidation ( $k_{\text{peco}}$ ). However, it is evident that after the concentration of methanol reaches a certain value, the photocatalytic oxidation reaction, which is caused by the photogenerated holes, might take over the reaction rate control, leading to the decrease of the methanol concentration. Hence, controlling the methanol formation is an important step which must not be neglected to avoid any reverse process and also it is interesting to note that the high selectivity of the photoreduction product of methanol can be achieved by using a IR light source.

## 4 Conclusion

In this work, working electrodes based on PbS thin films on SiNWs/Si substrates were applied as photocathode in both water splitting and  $\text{CO}_2$  reduction reactions. The bandgap energy of PbS was calculated to be 0.56 eV which means that the obtained PbS particles were nanocrystallines. The impact of introducing the PbS nanoparticles was well established and evidenced. It was shown that the performance

toward water reduction of the photocathodes was influenced by the etching time duration during SiNWs preparation. The  $\text{CO}_2$  photoelectrocatalytic test showed that the PbS thin film on nanostructured Si exhibits a higher  $\text{CO}_2$  reduction in comparison with the flat Silicon. Suitable band alignment between PbS and SiNWs facilitated the rapid transfer of photogenerated electrons from the CB of SiNWs to the CB of PbS for selective PEC  $\text{CO}_2$  reduction to methanol. An effective separation of the charge carrier and their transport to the surface due to suitable positions of energy bands was verified by the band diagram of energy position of the PbS/Si. It was concluded that a  $\text{PbCO}_3$  film was formed on the surface of the SiNWs which prevented photocorrosion of the surface. Methanol was the main product produced from the  $\text{CO}_2$ RR confirming the applicability of the PbS/SiNWs/Si-based photocathode for PEC reduction of  $\text{CO}_2$ . In addition, the direct oxidation of nanocrystalline PbS could be a good method for direct preparation of d-orbital-filled Pb nanocrystals. The oxidation of PbS to Pb is not a drawback since nanocrystalline Pb is one of the universal electrocatalyst to produce formic acid as a primary product of  $\text{CO}_2$ RR in aqueous electrolytes.

**Acknowledgements** The authors gratefully acknowledge the financial support from the Directorate General for Scientific Research and Technological Development (DGRSDT-Algeria).

**Funding** There are currently no Funding Sources on the list.

**Data availability** My manuscript and associated personal data.

## Declarations

**Conflict of interest** The authors declare that they have no conflict of interest.

**Consent to participate** The authors consent to participate.

**Consent for publication** The authors give their consent for publication.

**Informed consent** Not applicable for that section.

**Research involving human participants and/or animals** Not applicable for that section.

## References

- Xiao Y, Qian Y, Chen A, Qin T, Zhang F, Tang H, Qiu Z, Lin BL (2020) An artificial photosynthetic system with  $\text{CO}_2$ -reducing solar-to-fuel efficiency exceeding 20%. *J Mater Chem A*. <https://doi.org/10.1039/D0TA06714H>
- Kamiya K, Fujii K, Sugiyama M, Nakanishi S (2021)  $\text{CO}_2$  electrolysis in integrated artificial photosynthesis systems. *Chem Lett*. <https://doi.org/10.1246/cl.200691>
- Chen Z, Zhang H, Guo P, Zhang J, Tira G, Kim Y, Wu YA, Liu Y, Wen J, Rajh T, Niklas J, Poluektov OG, Laible PD, Rozhkova

- EA (2019) Semi-artificial photosynthetic CO<sub>2</sub> reduction through purple membrane re-engineering with semiconductor. *J Am Chem Soc.* <https://doi.org/10.1021/jacs.9b05564>
4. Allam D, Cheknoun S, Hocine S (2019) Operating conditions and composition effect on the hydrogenation of carbon dioxide performed over CuO/ZnO/Al<sub>2</sub>O<sub>3</sub> catalysts. *Bull Chem React Eng Cat.* <https://doi.org/10.9767/bcrec.14.3.3451.604-613>
  5. Ampelli C, Genovese C, Errahali M (2015) CO<sub>2</sub> capture and reduction to liquid fuels in a novel electrochemical setup by using metal-doped conjugated microporous polymers. *J Appl Electrochem.* <https://doi.org/10.1007/s10800-015-0847-7>
  6. Rajeshwar K (1985) Materials aspects of photoelectrochemical energy conversion. *J Appl Electrochem.* <https://doi.org/10.1007/BF00617736>
  7. Parsapur RK, Chatterjee S, Huang KW (2020) The insignificant role of dry reforming of methane in CO<sub>2</sub> emission relief. *ACS Energy Lett.* <https://doi.org/10.1021/acsenergylett.0c01635>
  8. Noue T, Fujishima A, Konishi S (1979) Photoelectrocatalytic reduction of carbon dioxide in aqueous suspensions of semiconductor powders. *Nature.* <https://doi.org/10.1038/277637a0>
  9. Bockris JOM, Wess JC (1989) The photoelectrocatalytic reduction of carbon dioxide. *J Electrochem Soc.* <https://doi.org/10.1149/1.2097455>
  10. Cheng J, Zhang M, Wu G, Wang X, Zhou J, Cen K (2014) Photoelectrocatalytic reduction of CO<sub>2</sub> into chemicals using Pt-modified reduced graphene oxide combined with Pt-modified TiO<sub>2</sub> nanotubes. *Environ Sci Technol.* <https://doi.org/10.1021/es500364g>
  11. Xie S, Zhang Q, Liu G, Wang Y (2016) Photocatalytic and photoelectrocatalytic reduction of CO<sub>2</sub> using heterogeneous catalysts with controlled nanostructures. *Chem Commun.* <https://doi.org/10.1039/C5CC07613G>
  12. Chen P, Zhang Y, Zhou Y, Dong F (2021) Photoelectrocatalytic carbon dioxide reduction: fundamental, advances and challenges. *Nano Mater Sci.* <https://doi.org/10.1016/j.nanoms.2021.05.003>
  13. Wang L, Wei Y, Fang R, Wang J, Yu X, Chen J, Jing H (2020) Photoelectrocatalytic CO<sub>2</sub> reduction to ethanol via graphite-supported and functionalized TiO<sub>2</sub> nanowires photocathode. *J Photochem Photobiol A.* <https://doi.org/10.1016/j.jphotochem.2020.112368>
  14. Ueda Y, Takeda H, Yui T, Koike K, Goto Y, Inagaki S, Ishitani O (2015) A visible-light harvesting system for CO<sub>2</sub> reduction using a Ru(II)-Re(I) photocatalyst adsorbed in mesoporous organosilica. *Chemosuschem.* <https://doi.org/10.1002/cssc.201403194>
  15. Yadav RK, Lee JO, Kumar A, Park NJ, Yadav D, Kim JY, Baeg JO (2018) Highly improved solar energy harvesting for fuel production from CO<sub>2</sub> by a newly designed graphene film photocatalyst. *Sci Rep.* <https://doi.org/10.1038/s41598-018-35135-7>
  16. Proppe AH, Li YC, Guzik AA, Berlinguette CP, Chang CJ, Cogdell R, Doyle AG, Flick J, Gabor NM, Van Grondelle R, Schiffer SH, Jaffer SA, Kelley SO, Leclerc M, Leo K, Mallouk TE, Narang P, Schlau-Cohen GS, Scholes GD, Vojvodic A, Wing-Wah Yam V, Yang JY, Sargent EH (2020) Bioinspiration in light harvesting and catalysis. *Nat Rev Mater.* <https://doi.org/10.1038/s41578-020-0222-0>
  17. Xie B, Lovell E, Hao Tan T, Jantarang S, Yu M, Scott J, Amal R (2021) Emerging material engineering strategies for amplifying photothermal heterogeneous CO<sub>2</sub> catalysis. *J Energy Chem.* <https://doi.org/10.1016/j.jechem.2020.11.005>
  18. Mo Y, Wang C, Xiao L, Chen W, Lu W (2021) Artificial light-harvesting 2D photosynthetic system with iron phthalocyanine/graphitic carbon nitride composites for highly efficient CO<sub>2</sub> reduction. *Catal Sci Technol.* <https://doi.org/10.1039/D1CY00858G>
  19. Momeni MM, Ghayeb Y, Ghonchehi Z (2015) Visible light activity of sulfur-doped TiO<sub>2</sub> nanostructure photoelectrodes prepared by single-step electrochemical anodizing process. *J Solid State Electrochem* 19:1359–1366. <https://doi.org/10.1007/s10008-015-2758-2>
  20. Momeni MM, Mozafari AA (2016) The effect of number of SILAR cycles on morphological, optical and photo catalytic properties of cadmium sulfide–titania films. *J Mater Sci: Mater Electron* 27:10658–10666. <https://doi.org/10.1007/s10854-016-5163-4>
  21. Momeni MM, Ghayeb Y, Akbarnia M et al (2020) Successive ionic layer adsorption and reaction (SILAR) deposition of nickel sulfide on the Fe<sub>2</sub>O<sub>3</sub> nanotube for efficient photocathodic protection of stainless steel under visible light. *J Iran Chem Soc* 17:3367–3374. <https://doi.org/10.1007/s13738-020-01992-1>
  22. Ghayeb Y, Momeni MM, Mozafari A (2016) Effect of silver sulfide decorating on structural, optical and photocatalytic properties of iron-doped titanium dioxide nanotubes films. *J Mater Sci: Mater Electron* 27:11804–11813. <https://doi.org/10.1007/s10854-016-5321-8>
  23. Momeni MM, Taghinejad M, Ghayeb Y, Bagheri R, Song Z (2020) High-efficiency photoelectrochemical cathodic protection performance of the iron-nitrogen-sulfur-doped TiO<sub>2</sub> nanotube as new efficient photoanodes. *Mater Res Express* 7:086403. <https://doi.org/10.1088/2053-1591/abaeal>
  24. Momeni MM, Ghayeb Y, Hallaj A, Bagheri R, Song Z, Farrokhpour H (2019) Photoelectrochemical performances of Fe<sub>2</sub>O<sub>3</sub> nanotube films decorated with cadmium sulfide nanoparticles via photo deposition method. *Physica B* 554:57–63. <https://doi.org/10.1016/j.physb.2018.11.048>
  25. Zhang N, Long R, Gao C, Xiong Y (2018) Recent progress on advanced design for photoelectrochemical reduction of CO<sub>2</sub> to fuels. *Sci China Mater.* <https://doi.org/10.1007/s40843-017-9151-y>
  26. Latempa TJ, Rani S, Bao N (2012) Generation of fuel from CO<sub>2</sub> saturated liquids using a p-Si nanowire/n-TiO<sub>2</sub> nanotube array photoelectrochemical cell. *Nanoscale.* <https://doi.org/10.1039/c2nr00052k>
  27. Beeman JW, Bullock J, Wang H, Eichhorn J, Towle C, Javey A, Toma FM, Mathews N, Ager JW (2019) Si photocathode with Ag-supported dendritic Cu catalyst for CO<sub>2</sub> reduction. *Energy Environ Sci.* <https://doi.org/10.1039/C8EE03547D>
  28. Ding P, Hu Y, Deng J, Chen J, Zha C, Yang H, Han N, Gong Q, Li L, Wang T, Zhao X, Li Y (2019) Controlled chemical etching leads to efficient silicone bismuth interface for photoelectrochemical CO<sub>2</sub> reduction to formate. *Mater Today Chem.* <https://doi.org/10.1016/j.mtchem.2018.10.009>
  29. Hu YP, Chen FJ, Ding P, Yang H, Chen JM, Zha CY, Li YG (2018) Designing effective Si/Ag interface via controlled chemical etching for photoelectrochemical CO<sub>2</sub> reduction. *J Mater Chem A.* <https://doi.org/10.1039/C8TA05420G>
  30. Choi SK, Kang U, Lee S (2014) Sn-coupled p-Si nanowire arrays for solar formate production from CO<sub>2</sub>. *Adv Energy Mater.* <https://doi.org/10.1002/aenm.201301614>
  31. Dasog M, Kraus S, Sinelnikov R, Veinot JGC, Rieger B (2017) CO<sub>2</sub> to methanol conversion using hydride terminated porous silicon nanoparticles. *Chem Commun.* <https://doi.org/10.1039/C7CC00125H>
  32. Kaci S, Keffous A, Trari M, Menari H, Manseri A, Mahmoudi B, Guerbois L (2010) Influence of polyethylene glycol-300 addition on nanostructured lead sulfide thin films properties. *Opt Commun.* <https://doi.org/10.1016/j.optcom.2010.04.046>
  33. Bashkany ZA, Abbas IK, Mahdi MA, Al-Taay HF, Jennings P (2018) A self-powered heterojunction photodetector based on a PbS nanostructure grown on porous silicon substrate. *SILICON.* <https://doi.org/10.1007/s12633-016-9462-4>
  34. Du K, Liu G, Chen X, Wang Z (2015) PbS quantum dots sensitized TiO<sub>2</sub> nanotubes for photocurrent enhancement. *J Electrochem Soc.* <https://doi.org/10.1149/2.0661510jes>

35. Carrasco-Jaim OA, Ceballos-Sanchez O, Torres-Martínez LM, Moctezuma E, Gómez-Solís C (2017) Synthesis and characterization of PbS/ZnO thin film for photocatalytic hydrogen production. *J Photochem Photobiol A*. <https://doi.org/10.1016/j.jphotochem.2017.07.016>
36. Shaban M, Rabia M, Abd El-Sayed AM, Ahmed A, Sayed S (2017) Photocatalytic properties of PbS/graphene oxide/polyaniline electrode for hydrogen generation. *Sci Rep*. <https://doi.org/10.1038/s41598-017-14582-8>
37. Zhong H, Mirkovic T, Scholes GD (2011) Nanocrystal synthesis. *Compr Nanosci Technol*. <https://doi.org/10.1016/B978-0-12-374396-1.00051-9>
38. Popov G, Bačić G, Mattinen M, Manner T, Lindström H, Sepänen H, Suihkonen S, Vehkamäki M, Kemell M, Jalkanen P, Mizohata K, Räisänen J, Leskelä M, Koivula H, Barry ST, Ritala M (2020) Atomic layer deposition of PbS thin films at low temperatures. *Chem Mater*. <https://doi.org/10.1021/acs.chemmater.0c01887>
39. Rahmani N, Dariani RS, Rajabi M (2016) A proposed mechanism for investigating the effect of porous silicon buffer layer on TiO<sub>2</sub> nanorods growth. *App Surf Sci*. <https://doi.org/10.1016/j.apsusc.2016.01.075>
40. Taherkhani M, Naderi N, Fallahzad P, Javad Eshraghi M, Kolahi A (2019) Development and optical properties of ZnO nanoflowers on porous silicon for photovoltaic applications. *J Electron Mater*. <https://doi.org/10.1007/s11664-019-07484-0>
41. Kong Q, Kim D, Liu C, Yu Y, Su YD, Li YF, Yang PD (2016) Directed assembly of nanoparticle catalysts on nanowire photoelectrodes for photoelectrochemical CO<sub>2</sub> reduction. *Nano Lett*. <https://doi.org/10.1021/acs.nanolett.6b02321>
42. Kaci S, Keffous A, Hakoum S, Trari M, Mansri O, Menari H (2014) Preparation of nanostructured PbS thin films as sensing element for NO<sub>2</sub> gas. *App Surf Sci*. <https://doi.org/10.1016/j.apsusc.2014.03.190>
43. Kaci S, Keffous A, Hakoum S, Manseri A (2015) Hydrogen sensitivity of the sensors based on nanostructured lead sulfide thin films deposited on a-SiC: H and p-Si (100) substrates. *Vacuum*. <https://doi.org/10.1016/j.vacuum.2015.02.024>
44. Kaci S, Keffous A, Trari M, Mahmoudi B, Menari H (2011) Enhancement of blue spectral response intensity of PbS via polyethylene oxide-adding for the application to white LEDs. *Adv Mater Res*. <https://doi.org/10.4028/www.scientific.net/AMR.227.39>
45. Moulai F, Hadjersi T, Ifires M, Khen A, Rachedi N (2019) Enhancement of electrochemical capacitance of silicon nanowires arrays (SiNWs) by modification with manganese dioxide MnO<sub>2</sub>. SILICON. <https://doi.org/10.1007/s12633-019-0066-7>
46. Kaci S, Keffous A, Hakoum S, Makrani N, Kechouane M, Guerbous L (2012) Investigation of nc-PbS/a-Si<sub>1-x</sub>C<sub>x</sub>: H/pSi (1 0 0) heterostructures for LED applications. *Opt Mater*. <https://doi.org/10.1016/j.optmat.2012.05.031>
47. Fellahi O, Barras A, Pan GH, Coffinier Y, Hadjersi T, Maamache M, Szunerits S, Boukherroub R (2016) Reduction of Cr(VI) to Cr(III) using silicon nanowire arrays under visible light irradiation. *J Hazard Mater*. <https://doi.org/10.1016/j.jhazmat.2015.11.020>
48. Hecht HG (1976) The interpretation of diffuse reflectance spectra. *J Res Natl Bureau Stand A*. <https://doi.org/10.6028/jres.080A.056>
49. Chernyshova IV (2001) Anodic oxidation of galena (PbS) studied FTIR-spectroelectrochemically. *J Phys Chem B*. <https://doi.org/10.1021/jp0110253>
50. Gao MR, Xu YF, Jiang J, Yu SH (2013) Nanostructured metal chalcogenides: synthesis, modification, and applications in energy conversion and storage devices. *Chem Soc Rev*. <https://doi.org/10.1039/C2CS35310E>
51. Zhang Z, Liu C, Brosnahan JT, Zhou H, Xu W, Zhang S (2019) Revealing structure evolution of pbs nanocrystal catalysts in the electrochemical CO<sub>2</sub> reduction using in situ synchrotron radiation X-ray diffraction. *J Mater Chem A*. <https://doi.org/10.1039/C9TA06750G>
52. Zhao X, Gorelikov I, Musikhin S, Cauchi S, Sukhovatkin V, Sargent E-H, Kumacheva E (2005) Synthesis and optical properties of thiol-stabilized PbS nanocrystals. *Langmuir* 21:1086–1090. <https://doi.org/10.1021/la048730y>
53. Weng B, Qi MY, Han C, Tang ZR, Xu YJ (2019) Photocorrosion inhibition of semiconductor-based photocatalysts: basic principle, current development, and future perspective. *ACS Catal*. <https://doi.org/10.1021/acscatal.9b00313>
54. Paracchino A, Brauer JC, Moser JE, Thimsen E, Graetzel M (2012) Synthesis and characterization of high-photoactivity electrodeposited Cu<sub>2</sub>O solar absorber by photoelectrochemistry and ultrafast spectroscopy. *J Phys Chem C* 116:7341–7350. <https://doi.org/10.1021/jp301176y>

**Publisher's Note** Springer Nature remains neutral with regard to jurisdictional claims in published maps and institutional affiliations.

## Authors and Affiliations

L. Allad<sup>1,2</sup> · D. Allam<sup>2</sup> · K. Benfadel<sup>1</sup> · S. Kaci<sup>1</sup> · M. Leitgeb<sup>3</sup> · A. Ouerek<sup>1,2</sup> · A. Boukezzata<sup>1</sup> · C. Torki<sup>1</sup> · S. Bouanik<sup>1</sup> · S. Anas<sup>1</sup> · L. Talbi<sup>1</sup> · Y. Ouadah<sup>1</sup> · S. Hocine<sup>2</sup> · A. Keffous<sup>1</sup> · S. Achacha<sup>1</sup> · A. Manseri<sup>1</sup> · F. Kezzoula<sup>1</sup>

<sup>1</sup> Thin Films Surfaces and Interfaces Division, CMSI-CRTSE, Research Center On Semiconductor Technology for Energetic, 2BD Frantz Fanon, 7 merveilles, POB 140, Algiers, Algeria

<sup>2</sup> Laboratory of Applied Chemistry and Chemical Engineering, Sciences Faculty, LCAGC-UMMTO, Mouloud Mammeri University of Tizi Ouzou, Tizi Ouzou, Algeria

<sup>3</sup> Institute of Sensor and Actuator Systems, TU Wien, 1040 Vienna, Austria